This is a repository copy of *Global Small-Angle X-ray Scattering Data Analysis of Triacylglycerols in the α-Phase (Part II)*.

White Rose Research Online URL for this paper:
http://eprints.whiterose.ac.uk/138127/

Version: Accepted Version

vGlobal Small-Angle X-ray Scattering Data Analysis of Triacylglycerols in the α-Phase

(Part II)

Marjorie Ladd Parada[1+], Amin Sadeghpour[1,2+], Josélio Vieira[3], Megan Povey[1] and Michael Rappolt[1*]

[1]School of Food Science and Nutrition, University of Leeds, LS2 9 JT, Leeds, U.K.

[2]Center for X-ray Analytics, Department of Materials Meet Life, Empa, St. Gallen, Switzerland

[3]Nestlé, Product Technology Centre, York, U.K.

*Corresponding author: Michael Rappolt, School of Food Science and Nutrition, University of Leeds, LS2 9 JT, Leeds, U.K., e-mail: M.Rappolt@leeds.ac.uk, Tel: +44 (0)113 3431931.

+ These authors contributed equally to the paper.

ABSTRACT

The early stage crystallisation behaviour in a triacylglycerol mixture has been investigated on the nanoscale with a novel global small angle X-ray scattering analysis technique. This method has been tailored for the determination of the electron density profiles (EDP) replicating both, (i) the nanostructural texture of molten TAGs (refer to part I 'Global Small-Angle X-ray Scattering Data Analysis of Triacylglycerols in the Molten State' of this publication series), and (ii) the lamellar structure of the metastable α-polymorph. In a first stage, the α-phase scattering contribution alone was examined by classical Fourier analysis as well as by globally fitting the data, leading to practically identical EDPs. Based on these findings, we extended our analysis to the entire X-ray scattering contribution arising from molten TAGs and the solid α-phase fraction. Remarkably, the experimental and theoretical data agree very well, providing for the first time a detailed nanostructural understanding about the coexisting molecular assemblies. This allowed in turn, also to quantitatively determine the solid fat content (SFC) with X-ray scattering data. Our new theoretical approach for measurement of SFC is based on the global analysis of small angle scattering/diffraction patterns and the SFC-results are in good agreement with values obtained from other techniques such as NMR spectroscopy.

INTRODUCTION

Triacylglycerols (TAGs) are ubiquitous natural fats and are the primary component of many food and cosmetic products. They are known to crystallise monotropically developing at least three different polymorphs, namely the α-, β'-, and β-phase, in order of increasing stability.[1, 2] For food industrial applications, it is important to note, that the quality of the crystallized final product depends strongly on the predominance of the different polymorphs. For instance, in the manufacturing of dark chocolate, the purity of the β-phase (polymorph V form) dictates the preferred textural attributes such as glossy appearance, mould release, cooling in the mouth and proper snap.[3-5] Another parameter that influences the fat physical properties, and thus its functionality, concerns the fatty acid (FA) composition within the TAG molecule, for variations on the FA chain length, degree of unsaturation and FA position in the glycerol backbone[6-10] strongly impact the molecular packing. When a fat system contains a mix of saturated and unsaturated FAs, the number of polymorphic structures increases as the lamellar packing needs to accommodate both, saturated and unsaturated FA chains. Note, due to the number of C=C double bonds in unsaturated FAs, one or more kinks are apparent along the hydrocarbon chain. Such is the case in cocoa butter (CB), which is composed mainly of three types of TAGs, namely POP, POS and SOS (see abbreviation list).[11] The presence of the oleoyl chain results in the development of four to six polymorphic structures, of which – as mentioned above – only the β-V form is desirable in chocolate production.[12, 13] This explains the continuing interest of the confectionary industry in understanding the crystallisation processes, both in terms of thermodynamic-kinetic pathways and fat structure.

In terms of nanostructure, detailed information has been obtained from X-ray single-crystal studies.[14-17] Unfortunately, given the monotropic nature of TAGs, i.e., the inherent instability of the α- and β'-forms, such studies were restricted to the most stable polymorph only, i.e., the β-phase. Therefore, a different approach is required, when seeking to obtain structural information of the metastable polymorphs. Thus, Mykhaylyk and Hamley[18, 19] applied classical Fourier Transform (FT) analysis, a technique that is widely also applied for liquid crystalline model membrane systems,[20] for the determination of electron density profiles (EDPs) from small angle X-ray diffraction (SAXD) data. This allowed them to obtain information on the lamellar thickness and FA tilt angles of the different SOS polymorphs, as well as to propose packing motifs for the γ, α$_2$ and α$_1$ forms. Nevertheless, concerning the spatial resolution the published EDP of the α$_1$ phase must be taken with some care, since only the first three order Bragg peaks were recorded. However, in our study we can show, that contributions of the 4th and 5th order Bragg peaks to the EDP play only a very minor role. Importantly though, in our

study we not only exploit the SAXD data, but also analyse and model the diffuse scattering arising from the molten fraction of TAGs. This is of relevance as during the early stages of bulk crystallisation when the α-form develops, only a small proportion of the fat is crystalline, thus the majority of the scattering profile comes from the molten TAGs.

In this regard, Loisel et al. attempted to comprehend the molecular arrangement in the coexisting phase regime proposing a hypothetical model based on qualitative understanding from combined DSC and diffraction data.[21] Although they do not provide calculations to simulate diffraction patterns, they propose that the saturated fatty acids decorate the crystalline hard core in the TAGs molecular assembly, while the mono- and/or poly-unsaturated fatty acids adapt a liquid like structure and thus are believed to contribute to the diffuse X-ray scattering.

Other studies mainly focus on the determination of the polymorphs present at different crystallisation stages,[22-28] but disregard the role of coexisting molten TAGs. An exception concerns the small angle X-ray scattering (SAXS) based work of Dewettinck et al.,[25] who fitted the diffuse X-ray scattering arising from the liquid state of TAGs with a Lorentzian distribution; however, this was only done to roughly estimate the liquid to solid phase ratio in any given diffraction pattern. Structural information in previous publications provide a great deal of information on the crystalline polymorphs,[22-25, 29] but so far, there has not been an integrative approach for simulating the X-ray scattering from TAGs in the transition states.

In our first paper of this series (refer to part I 'Global Small-Angle X-ray Scattering Data Analysis of Triacylglycerols in the Molten State'), we focused on the structural characterisation of molten CB applying a global fitting approach of the diffuse SAXS data. This led to a detailed description of a molecular assembly model for the liquid state, which satisfactorily simulated the experimental data. Briefly, we proposed a 'back-to-back' arrangement of TAGs in the core of these assemblies with loosely attached TAGs in a second layer. We note, the assemblies in the liquid state have been interpreted to be laterally extended, i.e., to have a planar geometry, but we cannot exclude the self-assemblies in the liquid state to be wormlike as well (for a detailed discussion on the dimensionality of TAG nanoclusters in the molten state refer to Part I of this publication series).

In this work, we go a step further, demonstrating how the SAXS pattern arising from both the liquid and coexisting α-phase can be analysed in great detail. Concerning the α-phase of CB, a few resemblances to smectic phospholipid phases are evident. While the diffuse scattering originates from individual membrane layers, contributing to the form factor scattering, diffraction peaks arise due to the quasi-long range ordering of the lamella, and thus, are contributing to the structure factor scattering.[21] Firstly, Pabst et al. provided a global SAXS

analysis method dealing with phospholipid multilayers in the liquid state[30]. This approach not only provides structural membrane information, but also mechanical membrane properties are taken into consideration by modelling the stacking disorder of 2nd type and including membrane undulations in the description of the system[31-33]. Adapting the basic principles of this global analysis technique of SAXS data above, we were able to deduce for the first time a global X-ray scattering description of the meta-stable α-phase of TAGs. Finally, combining the models for the liquid state (part I) with the developed model of the α-phase, we provide a novel nanostructural portrayal of the coexisting molecular assemblies. Note, that as a by-product, we are now also able to quantitatively determine the solid fat content (SFC) from the X-ray scattering data.

MATERIALS AND METHODS

Sample Preparation

West African cocoa butter (provided by Nestlé, PTC, York, U.K.) was used without additional refining. A 1.5 mm disposable quartz capillary was filled with molten CB (at 50 °C) and sealed with wax and an outer layer of epoxy glue. Subsequently, the capillary was loaded into the temperature-controlled stage of the SAXSpace camera (Anton Paar GmbH, Graz Austria).

X-ray Scattering Measurements

SAXS (small angle X-ray scattering) measurements were performed with the SAXSpace instrument (Anton Paar GmbH, Graz, Austria) equipped with a Cu-anode that operates at 40 kV and 50 mA (λ = 0.154 nm). The X-ray radiation was collimated using Kratky-type optics, which provides a line focused beam with a size of 20 x 0.3 mm (length x height). The instrument comprises a temperature stage (TCStage 150, Anton Paar, Graz, Austria) for temperature control in a range from -30 to 150 °C (precision 0.1 °C). The scattering vector modulus, q, was calibrated with silver-behenate ($q = 4\pi/\lambda \sin(\theta)$ with 2θ being the scattering angle). The sample-detector distance used for the small angle measurements was 130 mm covering the angular scattering range of 0.07 $nm^{-1} \leq q \leq 8$ nm^{-1}. The 1D scattering patterns were recorded with a Mython micro-strip X-ray detector (Dectris Ltd, Baden, Switzerland). More details on the set-up can be found in reference.[34]

To obtain the α-polymorph, the sample was held at 50 °C for 10 minutes and cooled down to 20 °C at a rate of 0.5 °C/min. The sample was left to stabilise for 5 minutes prior to taking measurements with an exposure time of 20 minutes. The resulting patterns were background subtracted by considering the scattering profile of empty capillary. The simulated curves were smeared using the length profile of the X-ray beam prior for comparison with experimental data.

Electron Density Profile Determination by Classical Fourier Analysis

As a rule of a thumb, EDPs of lamellar lipid self-assemblies determined by the classical Fourier analysis, are of reasonable quality when diffraction orders can be recorded up to $q = 4.2$ nm^{-1} (referring to minimum d-spacing, $d_{min} = 1.5$ nm)[35]. However, when it comes to the recording of the α-phase diffraction pattern, commonly no more than 3 diffraction orders are recorded, not even at a high-brilliance synchrotron SAXS-beamline.[19] Nevertheless, the authors were recently capable of recording also a very weak fifth order peak at a 4th generation synchrotron source, which to the best of our knowledge has not been reported elsewhere (Figure S1, see SI). EDPs of the α-phase were constructed by standard procedures.[36] In brief, the Bragg diffraction peaks were fitted by a Lorentzian distribution function, the intensities were Lorentz corrected and finally the square root of the corrected intensities resulted in the form factor values, F_h. In case of centrosymmetric EDPs, the Fourier transform (FT) is obtained by the summation of cosine terms only[37]:

$$\Delta\rho(z) = \sum_{h=1}^{h_{max}} \pm F_h cos\left(\frac{2\pi z h}{d}\right) \tag{1}$$

where $\Delta\rho$ is the electron density contrast, h the Miller index (diffraction order) and d denotes the lattice spacing.

EDP Determination from Global Fitting Analysis

The scattered intensity from multi-layered structures can be expressed as:

$$I(q) = \frac{S(q)|F(q)|^2}{q^2} \tag{2}$$

where F(q) is the bilayer form factor and S(q) is the structure factor,[30] and the normalization of q^2 reflects the Lorentzian correction of the recorded intensity (for details see ref.[38]). The form factor is given by the FT of the electron density profile along the membrane normal (z-axis). In this work, we apply a simple 2-Gaussian model to describe the EDP[37], where the 'positive' Gaussian represents the glycerol backbone of TAGs and the 'negative' Gaussian the methyl trough region (Figure 2).
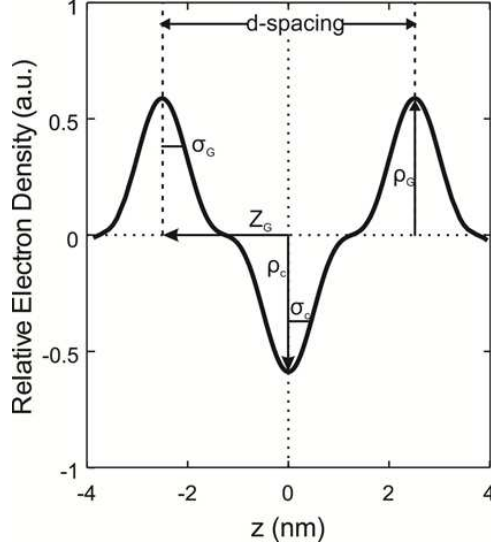
Figure 1. Applied two-Gaussian EDP model for the α-polymorph of CB. The 'positive' Gaussian at position $\pm z_G$ (width σ_G) with an amplitude of ρ_G represents the glycerol backbone region and the 'negative' Gaussian (width σ_C) centred at zero models the hydrocarbon chain region.

The form factor of the simple 2-Gaussian model becomes by FT:

$$F(q) = (2\pi)^{\frac{1}{2}} \left[2\sigma_G exp\left(-\frac{\sigma_G^2 q^2}{2}\right) cos(qz_G) - \sigma_C \rho_r exp\left(-\frac{\sigma_C^2 q^2}{2}\right) \right] \tag{3}$$

where z_G and σ_G represent the position and the width of the 'glycerol backbone', σ_C the width of 'hydrocarbon chain region' and $\rho_r = |\rho_C/\rho_G|$ is the ratio of the methyl trough to glycerol backbone contrast. Since the α-polymorph of CB is the least stable phase, we treated this polymorph alike to liquid crystalline phases of phospholipids with a the structure factor contribution based on the modified Caillé theory (MCT)[30, 39]:

$$S_{MCT}(q) = N + 2 \sum_{k=1}^{n-1} (N - k) cos(kqd) \cdot exp\left\{ -\left(\frac{d}{2\pi}\right)^2 q^2 \cdot \eta[\gamma + \ln(\pi k)] \right\} \tag{4}$$

where the mean number of scattering bilayers is identified as N, and γ is Euler's constant. The Caillé factor, η, describes the strength of disorder of second type in multi-layered structures and takes into account the bending rigidity modulus, K_C, and the bulk modulus for compression, B:

$$\eta = \frac{\pi k_B T}{2d^2 \sqrt{(BK_C)}} \tag{5}$$

Furthermore, from the resulting Caillé factor, the mean square fluctuation of the TAG-layers in the α-polymorph the can be estimated, following the equation proposed by Petrache et al.[40]:

$$\sigma^2 = \frac{\eta d^2}{\pi^2} \tag{6}$$

Finally, the experimental intensity data (Eq. 2) were globally fitted by using a Particle Swarm Optimization (PSO) approach[32] to avoid local minima fitting solutions.

Estimation of the Solid Fat Content

Crystallisation of TAGs is a dynamic process in which the arrangement of the molecules alters continuously over the cooling process or as time elapses. In fact, the α-polymorph of CB coexists always with fractions of molten TAGs that decrease over time as crystallisation progresses. The scattering pattern from such mixed phases is shown in Figure 2.
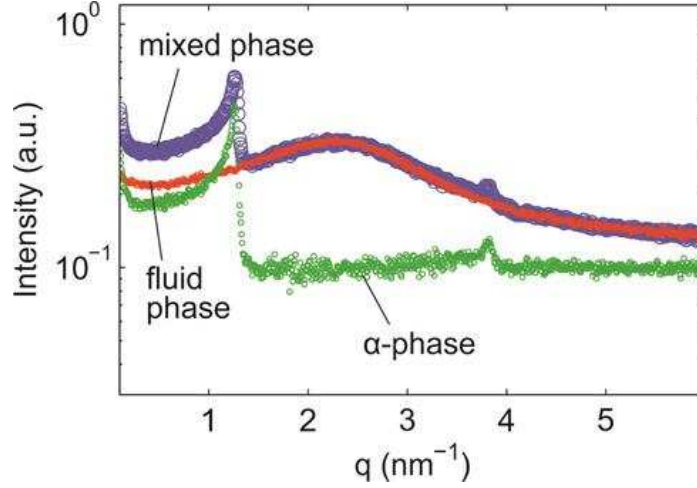

Figure 2. Small angle scattering curves of CB in fluid phase (red) obtained at 20 ºC (directly after the cooling ramp was completed) and the corresponding mixed fluid and α-polymorph (purple) obtained after 25 min at 20 ºC. The pure α-polymorph diffraction pattern (green) has been obtained in this case by subtraction of the fluid phase contribution from the mixed phase.

In the following, we shall briefly outline how the SFC can be estimated from the global small angle X-ray scattering analysis of the total intensity pattern (Figure 2, purple circles), that arises from (i) the molten TAGs (red dots) and (ii) α-phase contributions (green circles). Adding up these two contributions, we can express the total intensity as:

$$I(q) = \frac{1}{q^2}[(n_\alpha S(q)_\alpha |F(q)_\alpha|^2) + (1 - n_\alpha)|F(q)_m|^2)] \tag{7}$$

where n_α is a weighing factor for the contribution of the α-polymorph to the intensity profile, and $F(q)_\alpha$ and $F(q)_m$ (for $F(q)_m$ refer to part I, Eq. 11) are the form factors of the solid- and molten-state phases, respectively. We note, that the weighing factor n_α is not equivalent to the SFC, since the first term in equation 7 contains an additional structure factor contribution $S(q)_\alpha$ (Eq. 4). However, we can exploit the fact, that generally at q = 0 different form factor contributions to I(0) scale with their respective volumes[41], i.e., $(M_m/\rho_m)/(M_\alpha/\rho_\alpha) = F_m(0)^2/F_\alpha(0)^2$, where ρ_m and ρ_α are the densities of TAGs in the molten state and in the α-phase, respectively. Further, considering the experimentally determined weighing factors of each $F(0)^2$, we obtain for the solid fat content:

$$SFC = \frac{n_\alpha F(0)_\alpha^2}{n_\alpha F(0)_\alpha^2 + (1-n_\alpha)F(0)_m^2(\rho_m/\rho_\alpha)} \tag{8}$$

RESULTS AND DISCUSSIONS

Classical Electron Density Profile Determination of the α-Phase

In a first approach, we determined the electron density profiles (EDP) of the α-phase of CB at 20 °C from two different data sets, applying the classical FT approach (Eq. 2). Concerning the bench-top X-ray data, the highest recorded non-zero intensity concerned the 3rd order diffraction peak (see Figure 2 and 3), while with a fourth-generation synchrotron source, we were able to additionally to record a very weak 5th order diffraction peak (see SI, Figure S1). In Table 1, the diffraction data of the α-phase on CB (this work) and from Mykhaylyk and Hamley[19] on SOS are compared. Note, the best phase combinations for the given set form factors has been deduced from the continuous FT of our EDP model simulations (see subsequent section for further details). In agreement with Mykhaylyk and Hamley[19], we obtained -1,+1,-1 for the first three orders and -1 for the 5th order (note, the modelled 4th order amplitude is too low to allow a prediction of its phase value).

Table 1. Form factors, F_h, of CB in the α-phase at 20 °C (column 2 and 3) compared with the form factor values published for pure SOS at 20 °C.

h	F_h/F_1 (3-orders)	F_h/F_1 (5-orders)	F_h/F_1 (SOS[19])
1	-1.00	-1.00	-1.00
2	+0.00	+0.17	+0.15
3	-0.50	-0.63	-0.76
4	---	±0.00	---
5	---	-0.24	---

The resulting EDPs from the bench-top X-ray and synchrotron data were almost identical (Figure 4A and 4B). As listed in Table 2, both d-spacings are practically the same (4.93-4.94 nm) resulting in monolayer thickness of 2.47 nm, while the methyl trough and glycerol backbone thicknesses (σ_C and σ_G) are significantly larger for the SAXS bench-top data (0.08-0.12 nm difference; Table 2). However, the differences are very small, since the dominating electron density contrasts stem from the 1st and 3rd order peaks, while the 2nd order and 5th order electron density contrasts have only a minor impact on the final EDP (note, the 4th order electron density contrast has no influence on the final EDP).

Modelling of the Electron Density Profile of the α-Phase

By applying the global fitting method described in Eq. 2-4 to the scattering curve from the 'pure' α-phase contribution (Figure 3A; cp. also Figure 2), not only the EDP can be refined, but also the Caillé parameter is determined, indicating the inter-lamellar fluctuations.
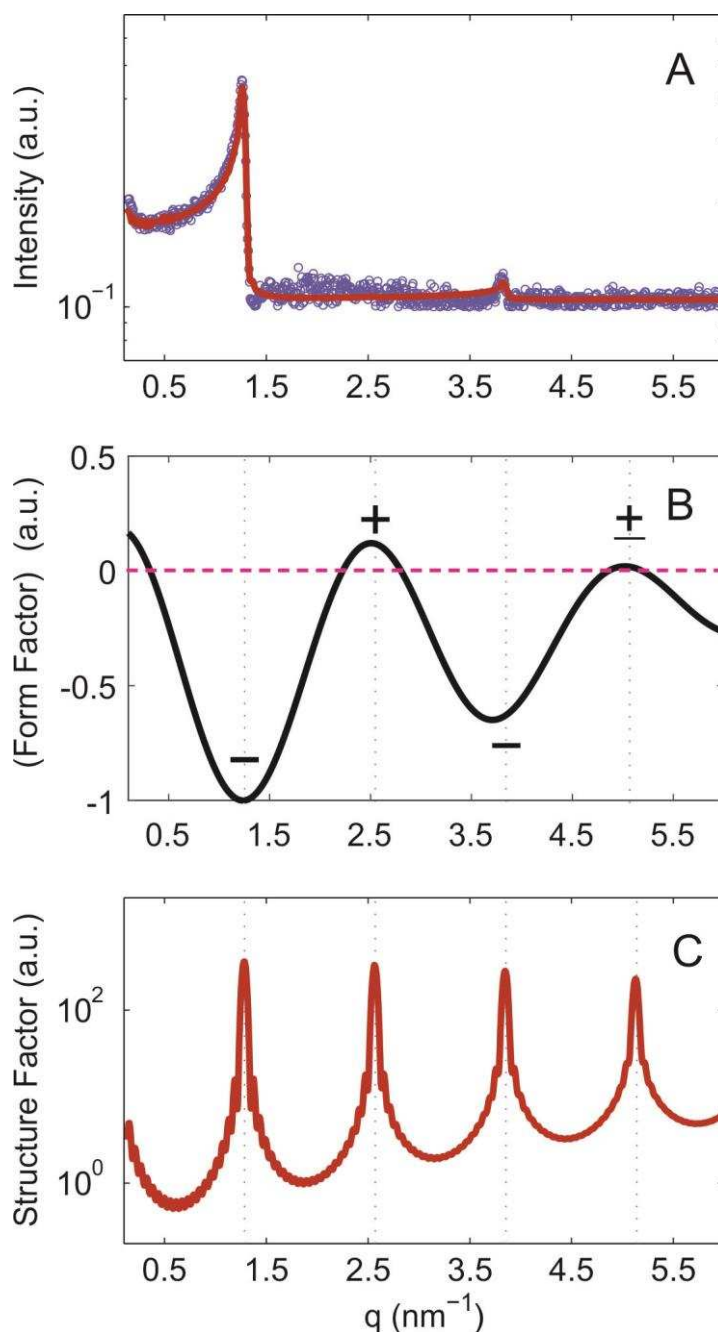

Figure 3. Global analysis of the SAXS data of the α-phase of CB at 20 °C. (A) Global fitting of the 'pure' α-phase contribution (cp. Figure 2), where the purple empty circles represent experimental data, and the red continuous line the best fit. (B) The corresponding continuous form factor plot is presented together with predicted phases. (C) The refined structure factor contribution determination based on the modified Caillé theory.[39]

Our analysis reveals that the d-spacing converges within experimental error to the same value (4.92 nm) as the ones obtained from FT analysis, consequently, the monolayer thickness

was found to be 2.46 nm. Moreover, the global SAXS analysis provides also similar σ_G and σ_C values (see Table 2). Plugging the obtained structural parameter values (Table 2) into Eq. 3 and plotting the continuous Fourier transform allows the prediction of expected phases (Figure 3B). As mentioned previously concerning the first five orders the expected best phase combination is -1, +1, -1, ±1 and -1.

The refined structure factor (Eq. 4) is displayed in Figure 3C. The Caillé fluctuation parameter was determined to be 0.01, which is about an order of magnitude smaller than values found in literature for multilamellar phospholipid bilayer systems in the liquid state.[31, 32] This is understandable for two reasons: (i) phospholipid bilayers are separated by water layers of the order of 2 nm, and hence bilayer undulations are less damped as compared to the TAG-layers in the α-phase, and (ii) the phospholipid bilayers in the liquid state are expected to display lower membrane bending rigidities as compared to the 2L-layers of the α-phase. The latter argument is supported by the fact the gauche to trans conformation ratio of the FA chains within α-polymorphs is significantly smaller as compared to phospholipid membranes in the liquid state.[42] We note, that for this reason, we also fitted the data with an alternative structure factor model, namely applying the paracrystalline theory of Hosemann,[43] originally developed to account for distortions in crystals. However, we could neither improve the goodness of our fittings nor was the outcome for the fluctuation parameter any different. In both cases, the derived mean fluctuations, σ, of the 2L-layers is about 0.15 nm (cp. Eq. 6; Table 2), thus representing layer undulations of about 3% of the d-spacing.

Table 2. Deduced structural parameters of CB in the α-phase at 20 °C. Results from classical Fourier Transform (FT) analysis are compared to results from the global fitting of the SAXS data.

Parameter	Classical FT (3 orders)	Classical FT (5 orders)	Global fitting
d-spacing (nm)	4.94±0.02	4.93±0.01	4.92±0.03
z_G (nm)	2.47±0.01	2.47±0.005	2.46±0.015
σ_G (nm)	0.36±0.14	0.28±0.11	0.22±0.13
σ_C (nm)	0.36±0.15	0.24±0.10	0.40±0.14
ρ_R[a]	1.00±0.12	0.82±010	1.00[a]±0.11
η	-	-	0.01±0.003
σ (nm)	-	-	0.15±0.05

[a]It is important to note, that the ρ_R values refer in this table to the final EDP of the stacked layers of TAGs; the TAG motif of a single layer displays a ρ_R value of 2.00 instead.
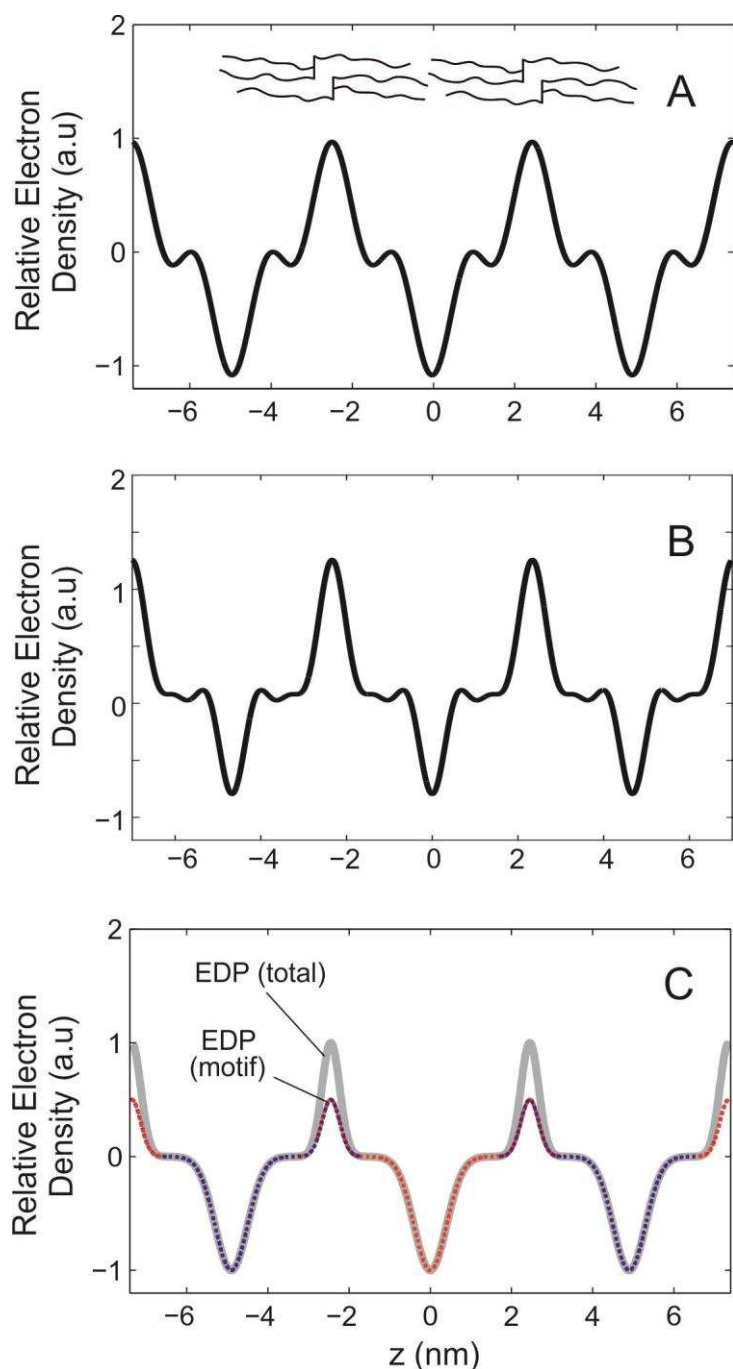
Figure 4. The electron density profiles calculated with (A) FT analysis from bench-top X-ray data (cp. Figure 3A), with (B) FT analysis from synchrotron-data (cp. Figure S1), and from C) the global fitting approach. The dashed lines in (C) represent the EDP motif obtained from the refinement of the EDP model of the α-phase and the solid grey line represents the resulting EDP of the stacking of TAG layers. Note, each single TAG layer practically fully overlaps at the position of the glycerol backbone with its nearest neighbour layer, i.e., the EDP of a single layer (motif) displays only half the electron density contrast at this position, when compared to the final EDP (total). In other words, the EDP motif (blue and red in panel C) includes only one-glycerol backbone on either side of the 2L layer, while the resulting EDP (grey) includes both glycerol backbones at this position reflecting correctly the back-to-back arrangement of the TAGs.

Global Fitting of Coexisting Liquid and α-Phases

In order to achieve a complete picture about the molecular arrangements at the early stages of crystallisation of CB, we can finally combine the two developed global fitting models for the liquid (part I) and solid state (this work). Applying Eq. 7 to our background-subtracted data of the α-phase scattering together with diffuse scattering arising from the molten TAGs, we obtain a perfect fit of the entire SAXS curve (Figure 5).
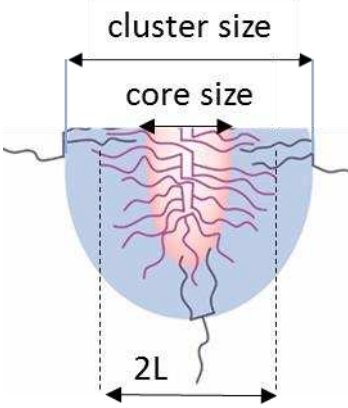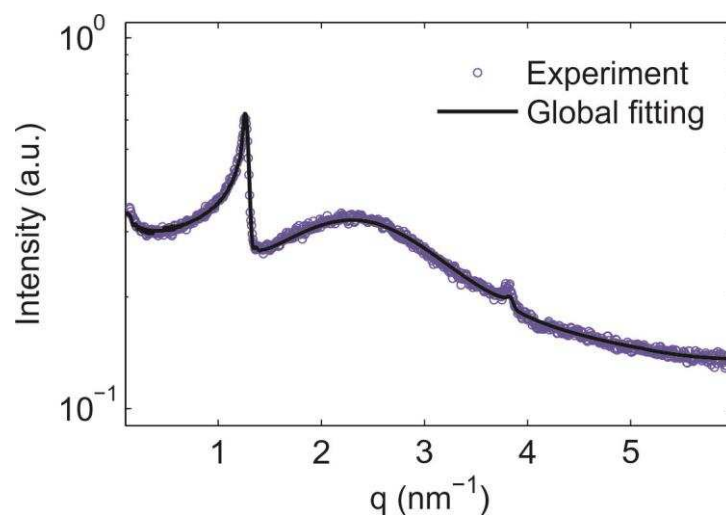

Figure 5. The SAXS data from cocoa butter at 20 °C and the corresponding global analysis with an obtained SFC of about 5%.

The main structural parameters of the α-phase result in a repeat distance of 4.92±0.03 nm, a glycerol backbone width of 0.22±0.13 nm and a methyl trough width of 0.40±0.14 (Table 2). We note, the overall d-spacing in the α-phase can be further decomposed into glycerol backbone and hydrocarbon core extensions. Since CB consists mainly of three different types of FAs (stearic: C18:0, palmitic: C16:0 and oleic: C18:1 acid) with oleic FAs having the shortest effective length and the stearic the longest, the average hydrocarbon extension compares well with the palmitic FA length. Assuming all *trans*-conformations in the FAs, leads to a thickness of the hydrocarbon core, d_C, of about 16 x 0.127 x 2 = 4.1 nm (note, a C-C bond length accounts for 0.127 nm[44]), that is, the glycerol backbone thickness is about 0.8 nm, which compares well to the fitted FWHM of the glycerol backbone thickness of 0.52±0.31 nm (Table 2).

These structural findings can now be compared with the refined structural parameters of the coexisting the molten TAG assemblies. Since the core TAGs and second layer TAGs do interdigitate according to our interpretation of the X-ray data fittings (see part I and the model scheme in Table 3), the overall extension of the fluid 2L layer core of the assemblies can only be estimated. Using the core and cluster size values, the 2L extension in the liquid state assembly is about (4.75-1.25) = 3.5 nm, which compares to 4.9 nm in the solid state of the α-

phase, i.e. $2L_{fluid}$ being about 1.3 nm thinner than $2L_{solid}$. This difference can be readily explained by the presence of *gauche* conformers in the FAs in the liquid state. We note, that precise measurements published on dipalmitoylphosphatidylcholine (DPPC) bilayers, display a similar overall hydrocarbon chain shortening of 2 x 0.6 = 1.2 nm, when comparing the solid lamellar phase at 20 °C with the fluid lamellar phase at 50 °C.[44]

Table 3. Deduced structural parameters of CB of molten TAG assemblies at 20 °C.

Parameter	Global fitting of assemblies in the liquid state	
Cluster size (nm)	4.75±0.06	cluster size
Core size (nm)	1.25±0.03	core size
Second layer occupancy (%)	16±1	2L

Finally, we are for the first time able to deduce directly the solid fat content (SFC) from the globally fitted X-ray data (cp. Eq. 8). After 5 minutes equilibration of the CB sample at 20°C, we obtained a SFC of about 5 %. For this we used the F(0)-values obtained from the global fitting analysis and literature values for the density of molten cocoa butter (904 kg/m^3 taken from the thesis of Ladd-Parada[45]) and the density α-polymorph (978 kg/m^3 taken from Lencki and Craven[46]). Our SFC value compare well with literature values obtained previously: Marrangoni et al.[47] (direct quenching), Dewettinck et al.[25] (direct quenching) and own pulsed-NMR[45] (step-wise cooling) led to values for the SFC from 9 to 11%, while Rigolle et al.[24] estimated the SFC = 5% from WAXS-data. The lower values from X-ray scattering when compared to the NMR data remain speculative, but it might be explained by the fact, that X-ray data are typically recorded faster than NMR data and hence might reflect earlier stages of formation of the α-polymorph.

CONCLUSIONS

Two novel EDP models have been developed to explain the scattering data of partially structured TAGs in the liquid state (part I) as well as to simulate the stacking of TAGs in α-polymorphs (this work). This allowed us for the first time, to obtain a complete structural picture of the cocoa butter in the early stages of crystallisation. The latter simulated findings are not only in excellent agreement with FT-analysis results, but allowed, moreover, the prediction of the correct phases of the experimental amplitudes as well as provided a first insight into the flexibility of the 2L-layers in the α-phase, i.e., small layer fluctuations of about 0.15 nm were determined.

Combining our two models, we further estimated for the first time the SFC directly from the SAXS data, which in our case accounted for 5% after 25 minutes of isothermal equilibration at 20 °C. Importantly, we can directly compare structural elements of molten TAG assemblies with the solid 2L-layered stacking of TAGs in the α-phase. The 2L back-to-back extension of TAGs in the liquid state has been estimated here to be 3.5 nm, which compares to a repeat distance of 4.9 nm in the α-phase. This difference is fully explained through all-trans conformations of the FAs within the α-phase, while trans-gauche conformations are dominant in the molten TAG assemblies. It is tempting to believe that the solidification of the proposed 4L-TAG-assemblies serve as first nucleation sites of the α-phase.

AUTHOR INFORMATION

Corresponding Author

Michael Rappolt

School of Food Science and Nutrition, University of Leeds, LS2 9 JT, Leeds, U.K.

E-mail: M.Rappolt@leeds.ac.uk

Tel: +44 (0)113 3431931

Author Contributions

The manuscript was written through contributions of all authors. All authors have given approval to the final version of the manuscript. [†]These authors contributed equally.

ABBREVIATIONS

CB, cocoa butter; TAG, triacylglycerol; FT, Fourier Transform; POP, sn-1,3-palmitoyl-2-oleoyl glycerol: POS, sn-1-palmitoyl-2-oleoyl-3-distearoyl glycerol SOS, sn-1,3-distearoyl-2-oleoyl glycerol; EDP, electron density profile; SFC, solid fat content; SAXS, small angle X-ray scattering; WAXS, wide angle X-ray scattering; FA, fatty acid; MCT, modified Caillé theory; pNMR, pulsed nuclear magnetic resonance.

TABLE OF CONTENTS IMAGE
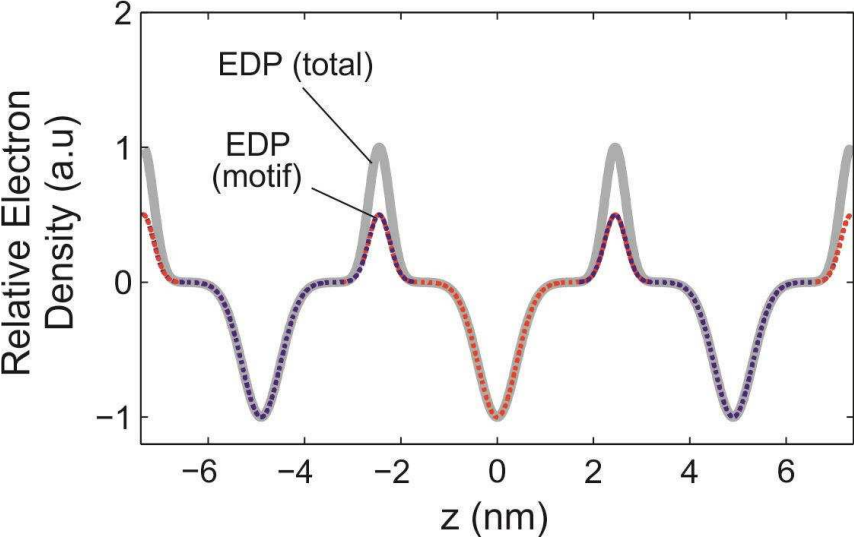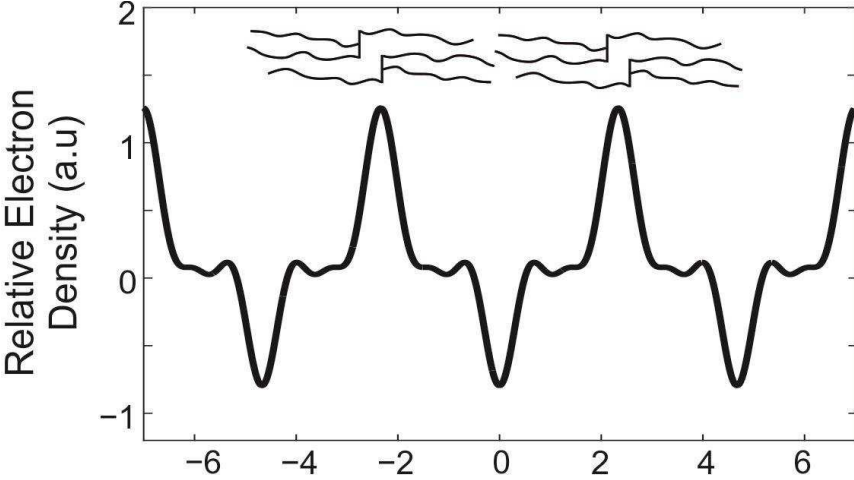
REFERENCES

1.   Koyano, T.; Hachiya, I.; Arishimo, T.; Sato, K.; Sagi, N., Polymorphism of POP and SOS. II. kinetics of melt crystallization. *J. Am. Oil Chem. Soc.* **1989,** 66, (5), 675-679.
2.   Koyano, T.; Hachiya, I.; Arishima, T.; Sagi, N.; Sato, K., Polymorphism of POS. II. kinetics of melt crystallization. *J. Am. Oil Chem. Soc.* **1991,** 68, (10), 716-718.
3.   Beckett, S. T., *Science of Chocolate*. The Royal Society of Chemistry: United Kingdom, 2000; p 127-142.
4.   Windhab, E. J., Tempering. In *Industrial Chocolate Manufacture and Use*, T.Becket, S., Ed. Wiley-Blackwell: United Kindom, 2007; pp 276-319.
5.   Talbot, G., Chocolate Temper. In *Industrial Chocolate Manufacture and Use*, 4th ed.; Becket, S. T., Ed. Blackwell Publishing, Ltd: Oxford, United Kingdom, 2009; pp 261-275.
6.   Lipp, M.; Anklam, E., Review of cocoa butter and alternative fats for use in chocolate—Part A. Compositional data. *Food Chemistry* **1998,** 62, (1), 73-97.
7.   Wille, R. L.; Lutton, E. S., Polymorphism of cocoa butter. *J. Am. Oil Chem. Soc.* **1966,** 43, (8), 491-496.
8.   Tascini, A. S.; Noro, M. G.; Chen, R.; Seddon, J. M.; Bresme, F., Understanding the interactions between sebum triglycerides and water: A molecular dynamics simulation study. *Physical Chemistry Chemical Physics* **2018,** 20, (3), 1848-1860.
9.   Takechi, C.; Kaneko, F., X-ray diffraction and vibrational spectroscopic study of the influence of cis- and trans-unsaturation on the α-phase of triacylglycerols. *J. Phys. Chem. B* **2013,** 117, (29), 8896-8905.
10.   Bayés-Garcia, L.; Calvet, T.; Cuevas-Diarte, M. A.; Ueno, S.; Sato, K., Phase behavior of binary mixture systems of saturated-unsaturated mixed-acid triacylglycerols: Effects of glycerol structures and chain-chain interactions. *J. Phys. Chem. B* **2015,** 119, (12), 4417-4427.
11.   Lipp, M.; Anklam, E., Review of cocoa butter and alternative fats for use in chocolate—Part B. Analytical approaches for identification and determination. *Food Chem.* **1998,** 62, (1), 99-108.
12.   MacMillan, S. D.; Roberts, K. J.; Rossi, A.; Wells, M. A.; Polgreen, M. C.; Smith, I. H., In Situ Small Angle X-ray Scattering (SAXS) Studies of Polymorphism with the Associated Crystallization of Cocoa Butter Fat Using Shearing Conditions. *Cryst. Growth Des.* **2002,** 2, (3), 221-226.
13.   Afoakwa, E. O.; Paterson, A.; Fowler, M.; Vieira, J., Influence of tempering and fat crystallization behaviours on microstructural and melting properties in dark chocolate systems. *Food Res. Int.* **2009,** 42, (1), 200-209.
14.   Vand, V.; Bell, I. P., A direct determination of the crystal structure of the [beta] form of trilaurin. *Acta Crystallographica* **1951,** 4, (5), 465-469.
15.   Van Langevelde, A.; Peschar, R.; Schenk, H., Structure of β-trimyristin and β-tristearin from high-resolution X-ray powder diffraction data. *Acta Crystallographica Section B* **2001,** 57, (3), 372-377.
16.   Van Langevelde, A.; Van Malssen, K.; Hollander, F.; Peschar, R.; Schenk, H., Structure of mono-acid even-numbered β-triacylglycerols. *Acta Crystallographica Section B* **1999,** 55, (1), 114-122.
17.   Culot, C.; Norberg, B.; Evrard, G.; Durant, F., Molecular analysis of the [beta]-polymorphic form of trielaidin: crystal structure at low temperature. *Acta Crystallographica Section B* **2000,** 56, (2), 317-321.
18.   Mykhaylyk, O. O.; Smith, K. W.; Martin, C. M.; Ryan, A. J., Structural models of metastable phases occurring during the crystallization process of saturated/unsaturated triacylglycerols. *J. Appl. Crystallogr.* **2007,** 40, (s1), s297-s302.

19.   Mykhaylyk, O. O.; Hamley, I. W., The Packing of Triacylglycerols from SAXS Measurements: Application to the Structure of 1,3-Distearoyl-2-oleoyl-sn-glycerol Crystal Phases. *The Journal of Physical Chemistry B* **2004,** 108, (23), 8069-8083.

20.   Tristram-Nagle, S.; Liu, Y.; Legleiter, J.; Nagle, J. F., Structure of Gel Phase DMPC Determined by X-Ray Diffraction. *Biophys.J.* **2002,** 83, (6), 3324-3335.

21.   Loisel, C.; Keller, G.; Lecq, G.; Bourgaux, C.; Ollivon, M., Phase transitions and polymorphism of cocoa butter. *Journal of the American Oil Chemists' Society* **1998,** 75, (4), 425-439.

22.   Van Malssen, K.; Peschar, R.; Brito, C.; Schenk, H., Real-time X-ray powder diffraction investigations on cocoa butter. III. Direct β-crystallization of cocoa butter: Occurrence of a memory effect. *JAOCS, Journal of the American Oil Chemists' Society* **1996,** 73, (10), 1225-1230.

23.   van Langevelde, A.; Van Malssen, K.; Peschar, R.; Schenk, H., Effect of temperature on recrystallization behavior of cocoa butter. *Journal of the American Oil Chemists' Society* **2001,** 78, (9), 919-925.

24.   Rigolle, A.; Goderis, B.; Van Den Abeele, K.; Foubert, I., Isothermal Crystallization Behavior of Cocoa Butter at 17 and 20 °C with and without Limonene. *Journal of Agricultural and Food Chemistry* **2016,** 64, (17), 3405-3416.

25.   Dewettinck, K.; Foubert, I.; Basiura, M.; Goderis, B., Phase Behavior of Cocoa Butter in a Two-Step Isothermal Crystallization. *Cryst. Growth Des.* **2004,** 4, (6), 1295-1302.

26.   Voda, A.; Den Adel, R.; Van Malssen, K.; Van Duynhoven, J., Quantitative Assessment of Triacylglycerol Crystallite Thickness by 1H Spin-Diffusion NMR. *Crystal Growth and Design* **2017,** 17, (4), 1484-1492.

27.   Schmiele, M.; Schindler, T.; Westermann, M.; Steiniger, F.; Radulescu, A.; Kriele, A.; Gilles, R.; Unruh, T., Mesoscopic structures of triglyceride nanosuspensions studied by small-angle X-ray and neutron scattering and computer simulations. *J. Phys. Chem. B* **2014,** 118, (29), 8808-8818.

28.   Verstringe, S.; Dewettinck, K.; Ueno, S.; Sato, K., Triacylglycerol crystal growth: Templating effects of partial glycerols studied with synchrotron radiation microbeam x-ray diffraction. *Crystal Growth and Design* **2014,** 14, (10), 5219-5226.

29.   Ikeda, E.; Ueno, S.; Miyamoto, R.; Sato, K., Phase behavior of a binary mixture of 1,3-dipalmitoyl-2-oleoyl-sn-glycerol and 1,3-dioleoyl-2-palmitoyl-sn-glycerol in n-dodecane solution. *J. Phys. Chem. B* **2010,** 114, (34), 10961-10969.

30.   Pabst, G.; Rappolt, M.; Amenitsch, H.; Laggner, P., Structural information from multilamellar liposomes at full hydration: Full q -range fitting with high quality x-ray data. *Physical Review E* **2000,** 62, (3), 4000-4009.

31.   Sanver, D.; Murray, B. S.; Sadeghpour, A.; Rappolt, M.; Nelson, A. L., Experimental Modeling of Flavonoid–Biomembrane Interactions. *Langmuir* **2016,** 32, (49), 13234-13243.

32.   Drasler, B.; Drobne, D.; Sadeghpour, A.; Rappolt, M., Fullerene up-take alters bilayer structure and elasticity: A small angle X-ray study. *Chemistry and Physics of Lipids* **2015,** 188, (0), 46-53.

33.   Rappolt, M.; Pabst, G., Flexibility and structure of fluid bilayer interfaces. In *Structure and dynamics of membranous interfaces*, Nag, K., Ed. John Wiley & Sons: Hoboken, 2008; pp 45-81.

34.   Patil-Sen, Y.; Sadeghpour, A.; Rappolt, M.; Kulkarni, C. V., Facile Preparation of Internally Self-assembled Lipid Particles Stabilized by Carbon Nanotubes. *Journal of visualized experiments* **2016,** (108).

35.   Rappolt, M., Bilayer thickness estimations with "poor" diffraction data. *Journal of Applied Physics* **2010,** 107, (8), -.

36.   Li, N. Y. D.; Perutková, Š.; Iglič, A.; Rappolt, M., My first electron density map: A beginner's guide to small angle X-ray diffraction. *Elektrotehniski Vestnik/Electrotechnical Review* **2017,** 84, (3), 69-75.

37.   Pabst, G.; Rappolt, M.; Amenitsch, H.; Laggner, P., Structural information from multilamellar liposomes at full hydration: full q-range fitting with high quality x-ray data. *Physical Review E* **2000,** 62, (3), 4000-4009.

38.   Warren, B. E., *X-ray Diffraction*. Addison-Wesley: Reading, 1969.

39.   Zhang, R.; Suter, R. M.; Nagle, J. F., Theory of the structure factor of lipid bilayers. *Physical Review E* **1994,** 50, (6), 5047-5060.

40.   Petrache, H. I.; Gouliaev, N.; Tristram-Nagle, S.; Zhang, R.; Suter, R. M.; Nagle, J. F., Interbilayer interactions from high-resolution x-ray scattering. *Physical Review E* **1998,** 57, (6), 7014-7024.

41.   Mylonas, E.; Svergun, D. I., Accuracy of molecular mass determination of proteins in solution by small-angle X-ray scattering. *J. Appl. Crystallogr.* **2007,** 40, (SUPPL. 1), s245-s249.

42.   Czamara, K.; Majzner, K.; Pacia, M. Z.; Kochan, K.; Kaczor, A.; Baranska, M., Raman spectroscopy of lipids: A review. *Journal of Raman Spectroscopy* **2015,** 46, (1), 4-20.

43.   Hosemann, R.; Bagchi, S. N., *Direct analysis of diffraction by matter*. North-Holland Publ. Co.: Amsterdam, 1962.

44.   Nagle, J. F.; Tristram-Nagle, S., Structure of lipid bilayers. *Biochimica Et Biophysica Acta-Reviews on Biomembranes* **2000,** 1469, (3), 159-195.

45.   Ladd-Parada, M. The effects of pressure and thermal history on the crystallisation of cocoa butter. Univsersity of Leeds, Leeds, 2018.

46.   Lencki, R. W.; Craven, R. J., Negative pressure induced cavity formation during cocoa butter crystallization. *JAOCS, Journal of the American Oil Chemists' Society* **2013,** 90, (10), 1509-1516.

47.   Marangoni, A. G.; McGauley, S. E., Relationship between crystallization behavior and structure in cocoa butter. *Crystal Growth and Design* **2003,** 3, (1), 95-108.